Surface electromagnetic wave excitation on one-dimensional photonic band-gap arrays

W. M. Robertson[a] and M. S. May
Department of Physics and Astronomy, Middle Tennessee State University, Murfreesboro, Tennessee 37132

(Received 7 August 1998; accepted for publication 2 February 1999)

Experiments are described on the prism-coupled excitation of surface electromagnetic waves in one-dimensional photonic band-gap arrays. The low loss of photonic band-gap materials leads to narrow angular reflectivity resonances and high surface fields. These attributes, coupled with the ability to engineer the optical properties of photonic band-gap arrays, suggest these materials as powerful replacements for metal films in many applications that make use of surface-plasmon resonance. © *1999 American Institute of Physics.* [S0003-6951(99)04313-2]

This letter describes experiments on the use of prism coupling to excite optical-frequency surface electromagnetic waves (SEWs) on one-dimensional photonic band-gap (PBG) arrays. The motivation for this work is twofold. First, techniques to measure the SEW dispersion in photonic band-gap arrays are important because many applications proposed for these materials can be impacted by the radiation channel due to surface modes.[1] A second reason for exploring SEWs in PBG materials is that these modes have the potential to be superior alternatives in many current applications to surface plasmons (SP) typically excited in metal films.

The general condition for the existence of SEWs at an interface between two media is that one material—the active medium—has a dielectric constant that is negative at the frequency of excitation, whereas the other medium is a pure dielectric. Under these conditions Maxwell's equations show that a propagating mode—evanescent in each medium—exists at the boundary.[2] For SP generation the active medium is typically a metal. The best results are obtained with metals such as aluminum, copper, gold, and silver, which have a negative real part of the dielectric constant and a small imaginary part indicative of low dielectric loss. In contrast, PBG materials are composed of a regular periodic arrangement of pure dielectrics. The activity of this composite medium results from the coherent effects of scattering and interference in the regular dielectric array that produces a material whose *effective* dielectric constant is negative. Loss in PBG systems, determined by the intrinsic loss of the constituents and interfacial roughness, is much lower than in metals.

Surface plasmons have a long history of use in areas such as nonlinear optics,[3,4] optical modulators,[5–7] and sensors.[8–12] SEWs on PBG materials offer potential advantages in many of these applications. First, the properties of the photonic crystal can be engineered to permit SEW excitation at virtually any optical frequency. This feature is valuable for optical SEW excitation in the blue/violet where most metals do not exhibit good characteristics for SP excitation. Second, the low dielectric loss in PBG arrays leads to much sharper resonant coupling between the incoming light and the SEW modes. Strong coupling results in much higher surface electromagnetic (EM) fields, beneficial for the excitation of surface nonlinear effects. Further, low loss produces much narrower reflectivity resonances in the prism reflectivity experiments, which leads to modulators with higher contrast ratios and sensors with significantly enhanced surface sensitivity.

Although much recent progress has been made on the fabrication of two- and three-dimensional dielectric arrays with photonic band gaps at optical frequencies, we chose to use one-dimensional PBG arrays because of the small size, fragility, and limited availability of higher-dimensional samples. The sample was fabricated commercially using conventional thin-film deposition and consisted of 15 bilayers of TiO_2/SiO_2 (30 layers total). The multilayer was designed to exhibit a photonic band gap over the frequency extent of the laser and within the angular range accessible by the prism reflection configuration. These constraints led to a multilayer consisting of alternating layers of 169.5 nm TiO_2 and 247.1 nm SiO_2 that corresponds to a quarter-wave Bragg reflector with a normal incidence stop band centered at 1.39 μm. At the angle of operation the band gap extended from 1 μm to just above 850 nm.

The experimental configuration for prism-coupled SEW excitation is shown in Fig. 1. The source is a tunable diode laser variable over the range from 835 to 863 nm. The multilayer was deposited on a glass substrate and the substrate was contacted to the prism using index-matching fluid.

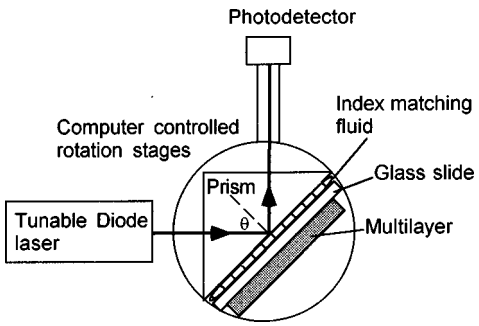

FIG. 1. Experimental configuration for surface wave generation using prism coupling.

[a]Electronic mail: wmr@physics.mtsu.edu

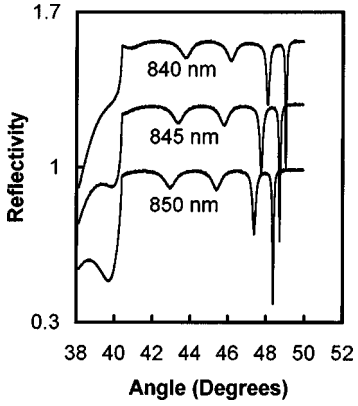

FIG. 2. Angular reflectivity plots for three different wavelengths. Top two traces have been displaced upward for clarity, thus the numerical scale is only correct for the lowest trace.

The prism and detector are mounted on two rotation stages, arranged coaxially, such that the detector tracks the movement of the reflected beam as the prism is rotated. The incident *s*-polarized laser beam is chopped and the photodetected signal is lock-in amplified and recorded by a computer-controlled data acquisition program.

Typical plots of the experimentally determined reflectivity as a function of incident angle at the reflecting face of the prism θ are shown in Fig. 2 for three wavelengths over the tuning range of the diode laser. The cusp at 40.3° in each case indicates the angle for total-internal reflection between the prism and the air. In each plot there are four reflectivity dips at angles greater than total-internal reflection. As described below, the deep, narrow dip (half-width 0.08°) at the largest angle corresponds to the excitation of a surface wave at the boundary between the dielectric stack and the air. The other three modes are guided waves confined within the PBG multilayer.

To understand the nature of the modes it is useful to consider a dispersion diagram that plots frequency against the surface component of the wave vector for the boundary between the multilayer and the air.[1] This diagram, shown in Fig. 3, can be divided into radiative and nonradiative regions. For example, on the air side of the film the radiative region at any frequency f exists from zero-wave vector up to a limiting value $2\pi f/c$. The limiting value corresponds to light traveling directly parallel to the interface—the largest wave vector possible for light of this frequency in air. In Fig. 3 the radiative region on the air side of the interface is indicated by the horizontal hatch lines and encompasses the region from the vertical axis to the light line. A similar procedure can be invoked to determine the limits of the radiative and nonradiative regions for light propagating in the multilayer photonic array. The problem is more complex because the response of the array varies with frequency and wave vector. To determine the radiative zones of our multilayer sample, we adapted the theoretical method described in Ref. 13. The diagonal hatching in Fig. 3 indicates radiative regions within the multilayer. Areas with no hatching correspond to frequency/wave-vector regions for which propagation in either medium is forbidden. Surface modes, confined to the interface, will exist in these parts of the dispersion diagram.

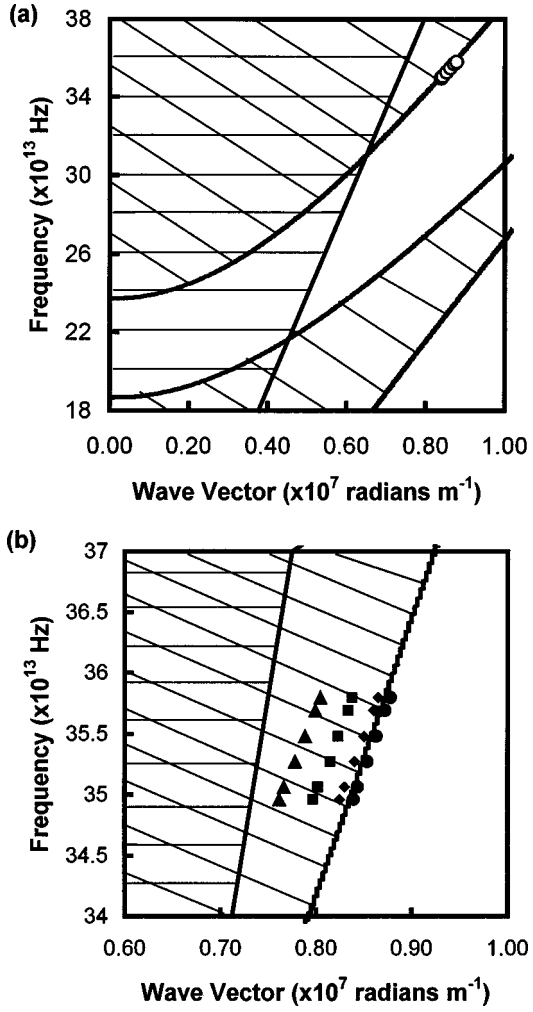

FIG. 3. (a) Surface wave dispersion diagram plotting frequency vs in-plane wave vector. The points are the experimentally determined values corresponding to the surface wave mode. (b) Detail of the experimentally explored part of the dispersion diagram showing that the surface mode lies in the nonradiative region, whereas the guided modes are radiative in the multilayer.

To categorize modes measured experimentally, we superpose the frequency and wave-vector values from the prism reflectivity experiment onto the dispersion diagram. The frequency of the mode is determined by the laser frequency, and the wave vector is derived from the parallel component of the prism-coupled light given by

$$k = \frac{2\pi f}{c} n \sin \theta_j , \tag{1}$$

where n is the refractive index of the prism, and θ_j is the angle of incidence at the respective reflectivity minima. In Fig. 3(a) only the largest wave-vector mode for each frequency is plotted on the dispersion diagram. These points lie in the nonradiative region, indicating that they correspond to an excitation bound to the surface.

Figure 3(b) shows an expanded view of the dispersion curve detailing the region of interest and plots all of the experimental modes at each frequency. Whereas the highest wave-vector mode lies in the nonradiative region, the lowest three modes at each frequency are confined to the diagonally hatched zone, indicating that the corresponding excitations

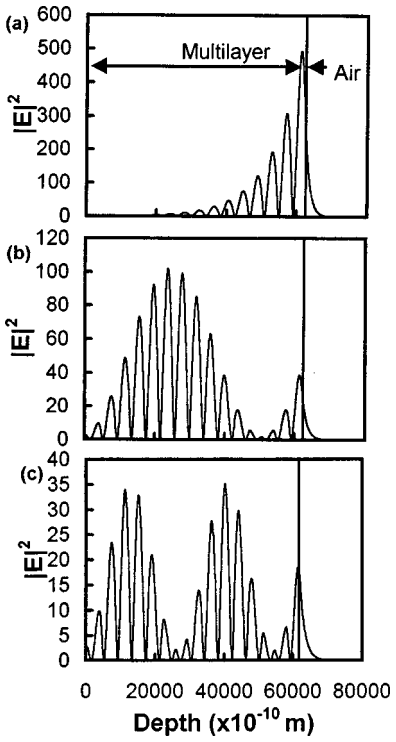

FIG. 4. Field profiles as a function of depth for (a) the surface wave, (b) the first guided mode, and (c) the second guided mode. The multilayer/air boundary is located at 6.3 μm.

are radiative in the multilayer. In fact, as the ensuing field analysis shows, these modes are guided excitations within the multilayer.

To highlight the difference between the surface mode and the guided modes, we present calculations of the squared *E*-field amplitude as a function of depth in the multilayer. The $|E|^2$ profiles were found by first calculating the prism reflectivity using Fresnel's equations, determining the angles of the reflectivity minima, and then solving for the field profile as a function of depth at each of these angles. Although Fresnel's equations predict a reflectivity similar to that measured, the angular positions of the guided modes, and more significantly, the angular width of the surface mode, do not match exactly with what is measured experimentally. The theoretically calculated surface mode has an angular reflectivity much narrower (half-width 0.01°) than that observed. This difference results because in the calculation we assume that the loss in the multilayer is determined solely by the intrinsic loss of each of the constituent layers. In fact, the loss is higher because of scattering introduced by the interfacial roughness between adjacent layers and at the surface.

With this caveat, the field calculations nonetheless illustrate nicely the difference between surface and guided modes. Figures 4(a), 4(b), and 4(c) show, respectively, the field profiles for the largest wave-vector (surface) mode, and for the next two lower wave-vector (guided) modes. The surface-mode field reaches its maximum in the first layer near the air interface. The field decays exponentially both into the air and into the multilayer. The conversion of the volume EM wave in the prism into the narrowly confined surface mode leads to a large field-enhancement (about 250× at the surface) characteristic of the SEWs. In contrast, the field profiles of the lower wave-vector modes have maxima that are confined within the multilayer. The first has one maximum and the second has two maxima. These field profiles are the first two standing-wave modes in the ''waveguide'' created by the multilayer.

In conclusion, our results show that it is possible to couple to SEW waves in PBG materials in the same optical configuration used in many SP applications. With the choice of sample parameters examined here, we observed a reflectivity half width of 0.08°—much narrower than that achievable with SPs in metal films (typically, 0.5°)—and corresponding to a $|E|^2$ enhancement of about 250 at the surface. SP field enhancements in metal films vary greatly with the choice of metal and the wavelength, but are typically less than 200. These findings suggest that PBG materials will play an important role in enhancing the capabilities of SEW devices.

This research was funded with a grant from the Research Corporation.

[1] R. D. Meade, K. D. Brommer, A. M. Rappe, and J. D. Joannopoulos, Phys. Rev. B **44**, 10961 (1991).
[2] E. N. Economou, Phys. Rev. **182**, 539 (1969).
[3] H. J. Simon, D. E. Mitchell, and J. G. Watson, Phys. Rev. Lett. **33**, 153 (1974).
[4] W. Knoll, M. R. Philpott, J. D. Swalen, and A. Girlando, J. Chem. Phys. **77**, 2254 (1982).
[5] O. Solgaard, F. Ho, J. I. Thackara, and D. M. Bloom, Appl. Phys. Lett. **61**, 2500 (1992).
[6] T. Okamoto, T. Kamitama, and I. Yamaguchi, Opt. Lett. **18**, 1570 (1993).
[7] M. E. Caldwell and E. M. Yeatman, Electron. Lett. **27**, 1471 (1991).
[8] H. E. de Bruijn, R. P. H. Kooyman, and J. Greve, Appl. Opt. **31**, 440 (1992).
[9] J. Gent, P. V. Lambeck, H. Kreuwel, G. Gerritsma, E. Sudhölter, D. Reinhoudt, and T. Popma, Appl. Opt. **29**, 2843 (1990).
[10] S. Löfas, M. Malmqvist, I. Rönnberg, E. Stenberg, B. Liedberg, and I. Lundström, Sens. Actuators B **5**, 79 (1991).
[11] K. Matsubara, S. Kawata, and S. Minami, Appl. Opt. **27**, 1160 (1988).
[12] E. Fontana, R. H. Pantell, and S. Strober, Appl. Opt. **29**, 4694 (1990).
[13] P. Yeh, A. Yariv, and C.-S Hong, J. Opt. Soc. Am. **67**, 423 (1977).